Journal of Molecular Liquids 295 (2019) 111713

Contents lists available at ScienceDirect

Journal of Molecular Liquids

journal homepage: www.elsevier.com/locate/molliq

Preparation of albumin nanoparticles in water-in-ionic liquid microemulsions

Begüm Demirkurt [a], Gulcin Cakan-Akdogan [b], Yasar Akdogan [a,*]

[a] Materials Science and Engineering Department, Izmir Institute of Technology, Izmir 35430, Turkey
[b] 1-Izmir Biomedicine and Genome Center, Izmir, 35340 Turkey 2-Department of Medical Biology, Faculty of Medicine, Dokuz Eylul University, Izmir, 35340 Turkey

ARTICLE INFO

Article history:
Received 28 June 2019
Received in revised form 3 September 2019
Accepted 6 September 2019
Available online 9 September 2019

Keywords:
Ionic liquids
Albumin nanoparticle
Microemulsion
Surfactant
High speed homogenization

ABSTRACT

Ionic liquids (ILs) with a variety of properties have been considered a unique class of solvents. Using ILs in microemulsions as oil substitutes provides environmentally benign media for various applications including nanoparticle synthesis. Here, bovine serum albumin nanoparticles (BSA NPs) widely used in drug delivery studies were prepared in nano-sized water droplets of water-in-IL (W/IL) microemulsion systems. A hydrophobic IL of 1-butyl-3-methylimidazolium hexafluorophosphate ($BmimPF_6$) was used as oil component in place of oils (castor oil, olive oil, etc.) and/or conventional organic solvents (cyclohexane, dichloromethane, etc.) in an emulsification method. In order to obtain spherical BSA NPs, high speed homogenizer treatment was applied followed by glutaraldehyde addition. Effects of glutaraldehyde, speed of homogenizer, type of surfactants and compositional fractions of the microemulsion components on the formation of water droplets and/or preparation of BSA NPs were studied using FTIR, EPR, DLS, and SEM techniques. Optimization of these preparation parameters showed that 3 wt% of BSA in a water/Tween 20/$BmimPF_6$ microemulsion with 20:50:30 wt% yielded ~100 nm average sized BSA NPs based on the SEM analysis. Although, water droplet size strongly depends on the water content, BSA nanoparticle size did not show a significant dependency on the water content. On the other hand, surfactant/IL weight ratio is more crucial for obtaining more uniformly size distributed albumin nanoparticles. A significant cellular uptake of BSA NPs prepared in IL based microemulsions with high cell viability showed the potential of this technique in preparation of albumin nanoparticles that can be used also in drug delivery studies.

1. Introduction

Over the past few decades, ionic liquids (ILs) composed of organic-inorganic ion pairs have been considered to be versatile and environmentally safe solvents that have application in many fields such as synthesis, catalysis, electrochemistry, and chemical industry [1–5]. Also, ILs have attracted extensive attention in microemulsion systems during recent years [6–9]. Several unique properties including good solvation ability, negligible vapor pressure, recyclability, low toxicity, high thermal stability, and a broad liquid temperature range make ILs suitable green alternatives to traditional toxic organic solvents [10–12]. In addition, ILs are called "designer solvents" since the cationic and anionic constituents of ILs can be modified to obtain desired properties in solutions [13]. Therefore, they have great potential applications in the microemulsion systems in which they can be used as each of the three components required to formulate a microemulsion e.g. substituted for oil, water, and surfactant molecules [6].

Microemulsions are formed by mixing two immiscible liquids with the help of surfactant molecules. They are thermodynamically stable and optically isotropic colloidal solutions. While they are homogenous in macroscale, formation of nano-sized droplets (5–100 nm size) of one in the other causes a microheterogeneous structure. Depending on the type and fraction of components, microemulsions are classified as water-in-oil (W/O), oil-in-water (O/W), and intermediate bicontinuous structural types. Water droplets are dispersed in a continuous phase of an oil in the W/O reverse microemulsions. On the other hand, oil droplets are dispersed in water in the O/W direct microemulsion. The size of droplets in microemulsion can be modified by the several parameters such as water content, type of surfactant (e.g. ratio of hydrophilic-lipophilic balance (HLB)), type of oil, and weight ratio of oil:surfactant. The use of droplets inside the microemulsions can be classified as a reaction medium for a variety of chemical reactions including nanoparticle synthesis. For example, nanoparticles based on metals (Au, Ag, Pt, Pd, Cu, etc.), bimetals (Pt/Pd, Ag/Au, Ag/Cu), metal oxides, semiconductors, polymers, and biomacromolecules have been prepared inside microemulsions [14–19].

* Corresponding author.
E-mail address: yasarakdogan@iyte.edu.tr (Y. Akdogan).

https://doi.org/10.1016/j.molliq.2019.111713
0167-7322/

ILs used as alternative substitutes in microemulsion systems have been utilized for nanoparticle preparations e.g. silica nanoparticles [19], latex nanoparticles [20], gold nanoparticles [21], and starch nanoparticles [17,22,23] in a limited number of studies. In our previous study, bovine serum albumin (BSA) protein was converted into nanoparticles (NPs) in a $BmimBF_4$ based microemulsion-like system [24]. Although water and $BmimBF_4$ are macroscopically miscible, their mixtures are not homogeneous on the microscopic scale especially for the water content around 50 mol% [25–27]. Thus, unstable mesostructures composed of water-rich and $BmimBF_4$-rich domains allow only formation of limited number of BSA NPs (200 nm average size) if specific compositional fractions of the microemulsion components, water/surfactant/IL, were used [24].

Serum albumin is the most abundant protein in the blood plasma of all vertebrates and serves as a carrier for various endogenous and exogenous compounds including fatty acids, steroids, ions, drugs [28]. Extensive drug binding ability of albumin inspired scientists to synthesize nanocarriers from albumin for drug delivery [29–34]. In addition, their unique properties such as biodegradability, lack of toxicity and antigenicity, and easy preparation make them a valuable candidate among all possible different nanocarriers [31]. Albumin nanoparticles can be prepared by emulsification method. Albumin aqueous solution was emulsified in an oil phase e.g. castor oil, cyclohexane or dichloromethane in the presence of surfactant molecules [35–37]. Applying a high-speed homogenizer, high-pressure homogenizer or ultrasonic shear followed by thermal heating or addition of a cross-linker produces stable albumin nanoparticles. BSA NPs with an average size of 600 nm were prepared in a water/SPAN-80/castor oil emulsion using an emulsion-heat stabilizing technique [35]. In another study, 400 nm average size BSA NPs were obtained in a water/SPAN-80/cyclohexane emulsion after applying a high speed homogenizer in the presence of glutaraldehyde as cross-linker [36]. Obtaining larger nanoparticles with emulsification method compared to the desolvation method limits using the method of emulsification. Moreover, using toxic and volatile organic solvents in both methods is harmful both for the environment and human health.

Differently, in this work, we used a hydrophobic IL of 1-butyl-3-methylimidazolium hexafluorophosphate ($BmimPF_6$) instead of using a conventional organic solvent in the emulsification method, which can provide a green medium with unique properties. Applying a high speed homogenizer followed by glutaraldehyde cross linking yielded BSA NPs. Experimental parameters which influence the BSA NP formation such as the weight ratios of microemulsion components, type of surfactant, homogenizer speed, and glutaraldehyde cross linking were studied in detail using Fourier transform infrared (FTIR) spectroscopy, dynamic light scattering (DLS), electron paramagnetic resonance (EPR) spectroscopy, and scanning electron microscopy (SEM). In addition, efficient cellular uptake of nanoparticles prepared in the IL microemulsion based system and their trivial effects on cell viability showed that the ionic liquid microemulsions have potential applications also for drug loaded nanoparticle preparation.

2. Experimental details

2.1. Materials

1-Butyl-3-methylimidazolium hexafluorophosphate ($BmimPF_6$), bovine serum albumin (BSA, Mw = 66,000 Da, lyophilized powder), fluorescein isothiocyanate labeled bovine serum albumin (FITC BSA), Tween 20, TX 100, glutaraldehyde solution (Grade II, 25% (v/v) in H_2O), absolute methanol and ethanol, 16-doxyl stearic acid (16-DSA), folic acid, N-(3-dimethylaminopropyl)-N′-ethylcarbodiimide hydrochloride, thiazolyl blue tetrazolium bromide (MTT), 2-(4-Amidinophenyl)-6-indolecarbamidine dihydrochloride (DAPI) were purchased from Sigma – Aldrich. Vybrant-DiI was purchased from Thermo All chemicals and solvents were analytical grade and used without any further purification. The pH of aqueous solutions was adjusted with 0.1 M NaOH or KOH for folic acid conjugation using an OHAUS STARTER3100 pH meter.

2.2. Preparation of W/IL microemulsions

The water/Tween 20/$BmimPF_6$ mixture forms microemulsions according to published works by Gao et al. [38] and Dong et al. [39] The ternary phase diagram was prepared and shown in Supplementary part, Fig. S1(A), which is very similar to the published results [38,39]. The three types of subregions in the microemulsion region e.g. W/IL, bicontinous and IL/W phases were determined by Gao et al. [38] using a cyclic voltammetry technique and by Dong et al. [39] using conductivity measurements. Here, subregions of the microemulsion were determined by conductivity measurements (Fig. S1(B–C)). We chose the specific compositions in the W/IL microemulsion region. Different compositions in the W/IL microemulsion region based on the ternary phase diagram were prepared. Components were mixed and listed according to their weight fractions (Table 1). In order to understand the effects of weight fraction of microemulsion components on the sizes of droplets and BSA nanoparticles, one component was kept constant and the others systematically were changed in the W/IL microemulsion region. By this way, sizes of water droplets and BSA nanoparticles can be monitored depend on different W:IL, W:surfactant and IL:surfactant ratios. First, $BmimPF_6$ and Tween 20 were mixed at 1200 rpm with magnetic stirrer for 15 min and then water was added into the IL-surfactant mixture. Stirring the mixture for 90 min at 1200 rpm yielded W/IL microemulsions with or without applying high-speed homogenizer at 22,000 rpm.

The ternary phase diagram of the microemulsion was prepared at 25 °C. After mixture of water and $BmimPF_6$, the Tween 20 was added into the solution until the solution became transparent, which was indicative of the formation of the single phase. A series of microemulsions were prepared through changing the weight ratio of water/$BmimPF_6$ at 9:1, 8:2, 7:3, 6:4, 5:5, 4:6, 3:7, 2:8, and 1:9, respectively. Conductivity measurements were taken with a portable conductometer (Thermo, Orion 3 Star) with a cell constant 0.475 cm^{-1}. The water was progressively added to the mixture of Tween 20 and $BmimPF_6$, and the conductance was measured after 2 min mixing and 30 min of waiting.

Table 1
Weights of water-in-IL microemulsion components prepared with different ratios.

Constant Tween 20 (g)				Constant IL ($BmimPF_6$) (g)				Constant water (g)			
Water	Tween 20	IL	wt%	Water	Tween 20	IL	wt%	Water	Tween 20	IL	wt%
0.050	1.250	1.200	2:50:48	0.050	1.950	0.500	2:78:20	0.125	2.125	0.250	5:85:10
0.125	1.250	1.125	5:50:45	0.125	1.875	0.500	5:75:20	0.125	1.875	0.500	5:75:20
0.250	1.250	1.000	10:50:40	0.375	1.625	0.500	15:65:20	0.125	1.250	1.125	5:50:45
0.500	1.250	0.750	20:50:30	0.575	1.425	0.500	23:57:20	0.125	0.875	1.500	5:35:60
0.750	1.250	0.500	30:50:20	0.750	1.250	0.500	30:50:20	0.125	0.500	1.875	5:20:75

2.3. Characterization of water droplets in the W/IL microemulsions

A series of ternary water/Tween 20/$BmimPF_6$ solutions with different wt% were measured by attenuated total reflectance Fourier transform infrared (ATR-FTIR) spectrometer (Perkin Elmer) with a resolution of 8 cm^{-1} and with a Malvern dynamic light scattering (DLS) Nano-ZS instrument (Worcestershire, UK). DLS was used for size measurements at a wavelength of 633 nm. The scattering angle was set at 173°.

2.4. EPR analysis of BSA:16-DSA complex in the W/IL microemulsions

Aqueous solution of 2 mM BSA in 0.1 M phosphate buffer (pH 7.4) and 26 mM 16-doxyl stearic acid (16-DSA) in 0.1 M KOH were prepared. The final concentrations of BSA and 16-DSA in the mixture are 0.75 mM and 1.5 mM, respectively. 16-DSA conjugated BSA solution before and after addition of $BmimPF_6$/Tween 20 mixture were measured with a CMS 8400 (Adani) benchtop X-band EPR spectrometer with a TE_{102} resonator cavity. Measurements were performed in quartz capillary sample tubes.

2.5. Preparation of BSA NPs in the W/IL microemulsions

BSA NPs were synthesized in the W/IL microemulsion systems with the help of high-speed homogenizer and glutaraldehyde as cross-linker. As an example, water/Tween 20/$BmimPF_6$ microemulsion with 10:50:40 wt% was prepared using 1 g of $BmimPF_6$ and 1.25 g of Tween 20. They were mixed at 1200 rpm with magnetic stirrer for 15 min. Then, 250 μL of 6% (w/v) BSA aqueous solution at pH = 9 was added dropwise to the IL/surfactant mixture. After 90 min of mixing, the system was stirred at 22,000 rpm for 2 min by high-speed homogenizer (IKA, T 18 TURRAX). At the end of homogenization, 45 μL of glutaraldehyde solution (Grade II, 25% (v/v) in H_2O) was added. The system was stirred overnight at 1200 rpm. Subsequently, albumin nanoparticles were precipitated with methanol under stirring at 1400 rpm followed by centrifugation at 15,000 rpm for 15 min. The pellet was washed with methanol, 50/50 (v/v) ethanol/water mixture and water to eliminate $BmimPF_6$, Tween 20, unreacted BSA and glutaraldehyde. Finally, pellets were prepared for characterizations. Experiments with different ratios from W/IL region of ternary phase diagram were performed based on the same procedure (Table 1).

2.6. Characterization of BSA NPs in the W/IL microemulsions

After centrifugation, pellets were dissolved in the same amount of ultrapure water. For scanning electron microscope (SEM, FEI QUANTA 250 FEG) analyses, nanoparticle solutions were diluted 100 times from their original volumes with ultrapure water. After that, 10 μL of nanoparticle solutions were dropped on an aluminum foil and samples were left in the fume hood for drying. Dried SEM samples were coated with gold using EMITECH K550X in a vacuum before SEM analyses. The accelerating voltage was 5 kV. Particle size analyses of SEM images were done by using ImageJ program. A Malvern dynamic light scattering (DLS) Nano-ZS instrument (Worcestershire, UK) was used for size measurements at a wavelength of 633 nm. The scattering angle was set at 90°.

2.7. Preparation of folate conjugated BSA NPs

BSA NPs, prepared as described above, were modified as the following method which is frequently used in the literature [40]. 800 μL of folic acid solution (20 mg/mL) in 0.1 M of $KOH_{(aq)}$ were incubated with 200 μL fresh N-(3-dimethylaminopropyl)-N-ethylcarbodiimide (EDC) under constant shaking in the dark for 15 min at 1400 rpm. Subsequently, 1 mL of BSA nanoparticle suspension (content 15 mg/mL) was added, and stirring continued for 1 h. Reaction was stopped by adding 100 μL hydroxylamine (500 mg/mL). The folate-conjugated nanoparticles were then purified from unreacted folic acid by 3 cycles of centrifugation (16,100 ×g, 10 min) and the pellet was dispersed to the original volume in water.

2.8. Cell uptake and imaging

Huh7 cells were cultured at 37 °C in presence of 5% CO_2 in DMEM containing penicillin/streptomycin and 10% FBS. For cell uptake test cells were labeled with DiI. 500,000 cells were washed with PBS and incubated in 50 μL PBS containing 2.5 μL DiI 20 min in 37 °C incubator, washed once with FBS, twice with PBS and resuspended in 5 mL complete DMEM, 50,000 cells/well were seeded in 8-well chamber slides (SPL). Next day 0.1 mg/mL FITC-BSA NPs were added via medium replacement and incubated 4 h or 24 h for uptake test. Cells were washed with PBS, fixed with 4% PFA, washed with PBS and nuclei was stained with 4 μg/mL DAPI solution for 5 min, slides were mounted with 80% glycerol. Slides were imaged with Zeiss LSM880 Confocal microscope using 63× oil objective, Z stacks with 3 μm slices were taken to check whether NPs are in the cells. Image processing is done with FIJI software.

2.9. Cell viability assay

Cell viability was assessed with MTT assay as follows: Cells were seeded on 96-well plates at 7000 cells/well, incubated overnight for adherence. 20 mg/mL BSA NP suspensions were prepared in sterile PBS and added to complete DMEM at a final concentration of 4 mg/mL. Serial dilutions of BSA NPs were made with complete DMEM to obtain final concentrations of 2 mg/mL - 0.05 mg/mL, and cells were incubated with the NP containing DMEM for 24 h and 48 h. Control cells were treated with PBS in corresponding volumes. For MTT test, 15 μL of 5 mg/mL MTT was added to 100 μL of DMEM, cells were incubated with this mix for 4 h. Cell medium was aspirated and 100 μL DMSO was added to each well to dissolve formazan, incubated at RT in dark for 30 min. Photometric measurements were recorded at 570 nm with Thermo Multiskan GO plate reader. Each measurement was done in 3 replicas, and % viability was calculated.

3. Results and discussion

In this study, a hydrophobic ionic liquid, $BmimPF_6$, was used as oil phase for the microemulsion formulation. $BmimPF_6$ was selected since it is a water immiscible ionic liquid, the maximum solubility of water in $BmimPF_6$ was found to be between 1.2 and 2.3 wt% [41], and it has less toxicity compared to other hydrophobic ionic liquids (e.g. $BmimNTf_2$) [42]. Also, formation of stable microemulsion water droplets in the $BmimPF_6$ continuous phase has already been obtained in the presence of Tween 20 as a surfactant [38,39].

Fig. 1 shows the photographs of different water/$BmimPF_6$ mixtures. After addition of water to $BmimPF_6$ (20:80 wt%, water:$BmimPF_6$), a phase separation took place in a few seconds (Fig. 1(A)). On the other hand, addition of 50 wt% of Tween 20 to the mixture of water/$BmimPF_6$ reduced the interfacial tension between water and $BmimPF_6$, and formed a transparent solution (Fig. 1(B)). Obtaining the single phase transparent solution indicates the formation of microemulson. In the W/IL microemulsion, water droplets were well dispersed in the continous IL phase with the help of Tween 20. The nano-sized water droplets/pools obtained in the microemulsion systems can be used as nanoreactors to synthesize nanoparticles. In this study, BSA protein nanoparticles were prepared inside the water droplets of the W/IL microemulsion system with the help of high-speed homogenizer and glutaraldehyde as cross-linker (Fig. 1(C)). The weight fraction of water is an important determinant for the size and stability of obtained water pools. Therefore, at first, effects of various fractions of microemulsion components on the formation of water droplets were studied with FTIR and DLS techniques.

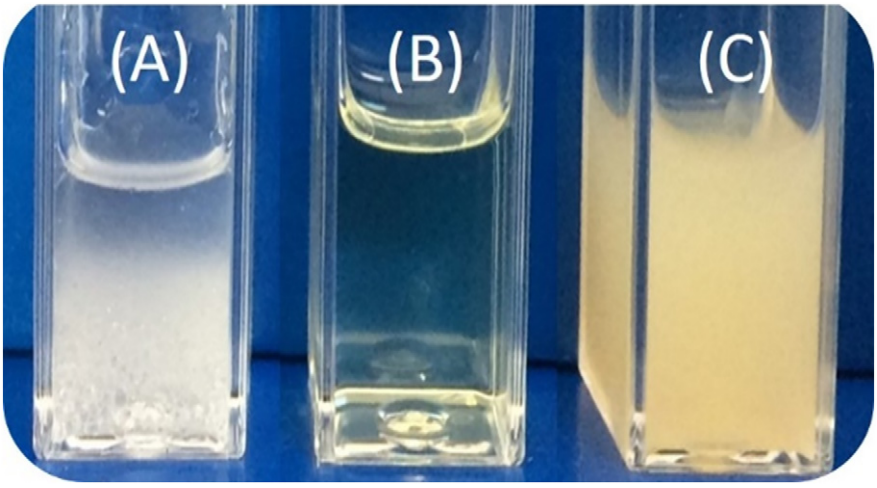

Fig. 1. Photographs of (A) water/$BmimPF_6$ heterogenous mixture with 20:80 wt%, (B) water/Tween 20/$BmimPF_6$ microemulsion with 10:50:40 wt% and (C) synthesized BSA NPs in the (B) with the help of high-speed homogenizer and glutaraldehyde.

3.1. Characterization of water droplets in the W/IL microemulsions

Infrared spectroscopy can be used to study water droplets in microemulsions [10,43]. Fig. 2 shows the formation of water droplets at different water contents while keeping the surfactant concentration constant. Five different compositions were chosen in the W/IL micromulsion region based on the ternary phase diagram in the presence of 50 wt% of Tween 20 (Table 1 and Fig. S1). Distinguishing O—H stretching frequencies of water signals come from bulk (nano-sized water droplets) and free (dispersed in IL/surfactant) water molecules allows monitoring nano-sized water droplet formation with IR spectroscopy [10]. Fig. 2(A) shows IR spectra of the microemulsion components e.g. $BmimPF_6$, Tween 20 and water. For $BmimPF_6$, C—H stretching frequencies of alkyl groups and imidazolium ring were observed explicitly in 2800–3015 cm^{-1} and in 3090–3225 cm^{-1}, respectively.

Also, a trace amount of water was detected in $BmimPF_6$ with O—H stretching frequencies at 3589 and 3677 cm^{-1} [43]. On the other hand, Tween 20 and water have broad signals in the region of 3300–3680 cm^{-1} and 3000–3700 cm^{-1}, respectively, due to the O—H stretching vibrations.

Fig. 2(B) showed the IR spectra of the microemulsions composed of 2, 5, 10, 20 or 30 wt% of water in $BmimPF_6$ with 50 wt% of Tween 20. The O—H stretching band (3200–3700 cm^{-1}) was normalized to enable comparison between the samples. The signals at 3594 and 3642 cm^{-1} were originated from the individual water molecules dispersed (free) inside the $BmimPF_6$/Tween 20 network. Increasing the water content decreased the intensities of dispersed water signals, and they disappeared eventually. In contrast, a new signal appeared at 3260 cm^{-1} was not detected in the $BmimPF_6$/Tween 20 mixture. Intensity of this signal increased with water content, and also it was observed in the spectrum of water. Therefore, signal at 3260 cm^{-1} was assigned to the bulk water formed inside the microemulsion.

In a FTIR spectrum, overlapped bands can be resolved from one another with a deconvolution method. Therefore, deconvolution can be applied in Fig. 2(B) to the mixtures of water:Tween20: $BmimPF_6$. In order to identify the dispersed (free) water (3594 and 3642 cm^{-1}) and bulk water (3260 cm^{-1}) bands, Fig. S2 showed the deconvoluted spectra belong to the mixture of $BmimPF_6$ and Tween 20 (no additional water), and water/Tween 20/$BmimPF_6$ microemulsion at 10:50:40%wt ratio. Deconvolution revealed the signals at 3260, 3594 and 3642 cm^{-1}.

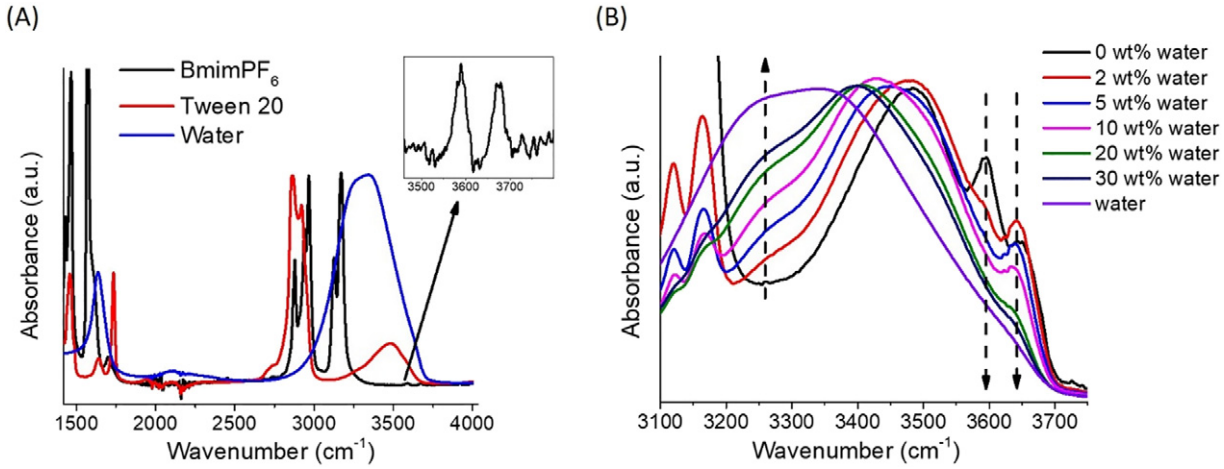

Fig. 2. (A) ATR-FTIR spectra of microemulsion components: $BmimPF_6$, Tween 20 and water. Inset shows the presence of residual dissolved water molecules in $BmimPF_6$. (B) O—H stretching band region of different water/$BmimPF_6$ microemulsions in the presence of constant 50 wt% of Tween 20. Up-arrow shows the formation of bulk water and down-arrows show the reducing amount of dispersed water in the system.

In order to further confirm the formation of nano-sized water droplets and also to determine the size of them, the same W/IL microemulsion systems measured with IR spectroscopy were studied with dynamic light scattering (DLS or photon correlation spectroscopy, PCS) technique. In microemulsions, hydrodynamic radii of water swollen micelles and oil swollen micelles can be characterized by DLS technique [10,44,45]. Light is scattered from the droplets and the scattering intensity oscillates due to the Brownian motion of the droplets in microemulsion. DLS detects the diffusion rate of droplets in solution using the fluctuations of the scattering intensity. The Stokes-Einstein equation can be used to convert the diffusion coefficient (D) to determine the hydrodynamic radius (R_h) of the scattering droplet:

$$Rh = \frac{kT}{6\pi\eta D}$$

where k is the Boltzmann constant, T is the absolute temperature, and η is the viscosity of the continuous phase.

Fig. 3(A) and (B) shows the effects of the water content and the homogenizer treatment on the size of water droplets formed in microemulsions. DLS measurements of water pools formed in different water/$BmimPF_6$ microemulsions at a constant Tween 20 concentration (50 wt%) were done using pH = 9 water after 1 h and 48 h sample preparations. The DLS results did not change with time. Therefore, using water at pH 9 did not affect the stability of the microemulsion.

At low water contents such as 2 and 5 wt%, the sizes of water droplets are around 20 nm. Applying high-speed homogenizer reduced the average sizes of water droplets to around 12 nm via mainly turbulence mechanism. Also, narrow size distributions were obtained both before and after applying homogenizer. However, at higher water contents, the size of water droplets increased and its size distributions broadened, significantly.

The average size of water droplets increased from 20 nm to 42, 78, and 105 nm when 10, 20 and 30 wt% of water were used, respectively. Similar to other reported microemulsions, swelling of water droplet took place with increasing the water content [10,44]. Also at 30 wt% of water, the size distribution changed from 68 nm to 180 nm. At higher water contents, homogenizer treatment also reduced the size of water droplets but did not narrow the size distribution. These showed that water droplet size and its size distribution strongly depend on the water concentration but not to homogenizer treatment in the same way. The Fig. 3(B) shows the water droplets swelling behaviour depends on the water to surfactant mass ratios (R value). For the both cases, with and without homogenizer treatment, there is a nearly linear correlation between the R values and the size of droplets indicating a spherical shape of water droplets formed in the W/IL microemulsions [46]. This shows that applying the high-speed homogenizer to the system did not damage the shape of water droplets.

3.2. Preparation of BSA NPs in the W/IL microemulsions

BSA NPs were prepared in the W/IL microemulsion systems (Table 1 and Fig. S1) with the help of high-speed homogenizer and glutaraldehyde as cross-linker. At first, the pH of BSA aqueous solution was adjusted to 9.0 in order to increase the absolute value of charge on the albumin. At pHs 7.0 and 9.0, the reported charges of BSA are −13 and −26, respectively [47]. The absolute value of charge of BSA at pH 9.0 is twice that of BSA at pH 7.0. The higher net charge on the BSA results in the higher electrostatic repulsive forces which avoid the agglomeration of albumin nanoparticles at the very beginning of the nanoparticle synthesis [24]. Addition of BSA aqueous solution to $BmimPF_6$/Tween 20 mixture was accompanied by significant denaturation of protein. Electron paramagnetic resonance (EPR) spectroscopy was applied to investigate the protein denaturation in the prepared microemulsion systems. Spin labeled fatty acid, 16-doxylstearic acid (16-DSA), was mixed with BSA at a 2:1 ratio (16-DSA/BSA) to obtain information on the protein structure [48–50]. Fig. 4(A) shows the continuous wave (CW) EPR spectrum of the 16-DSA in the aqueous BSA solution at room temperature. Broad outer hyperfine features originating from the restricted rotational motion showed that 16-DSAs were bound to BSA in buffer solution. However, sharper EPR signals were observed when different W/IL microemulsion formulations were added to the 16-DSA/BSA conjugation (Fig. S3). Fig. 4(B) shows the EPR spectrum of 16-DSA/BSA conjugation in the water/Tween 20/$BmimPF_6$ microemulsion system with wt%

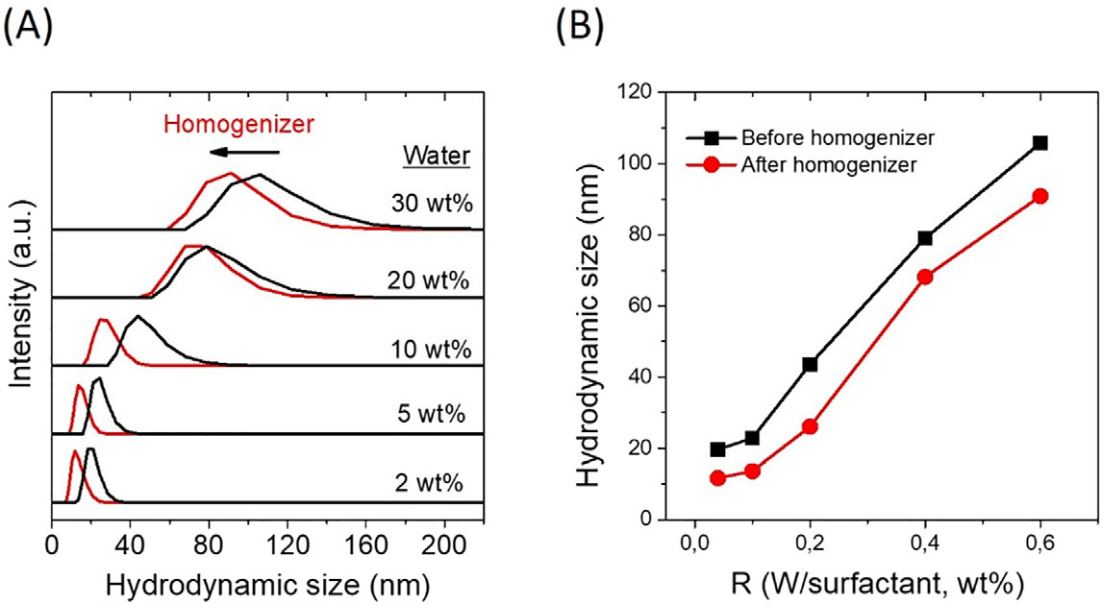

Fig. 3. (A) DLS results of water pools formed in different water/$BmimPF_6$ microemulsions at a constant Tween 20 concentration (50 wt%) (black) and after high-speed homogenizer treatment at 22,000 rpm (red). (B) Dependence of hydrodynamic size of water pools on R value (water/surfactant, wt%) in the microemulsion before (black) and after homogenization (red) at 22,000 rpm.

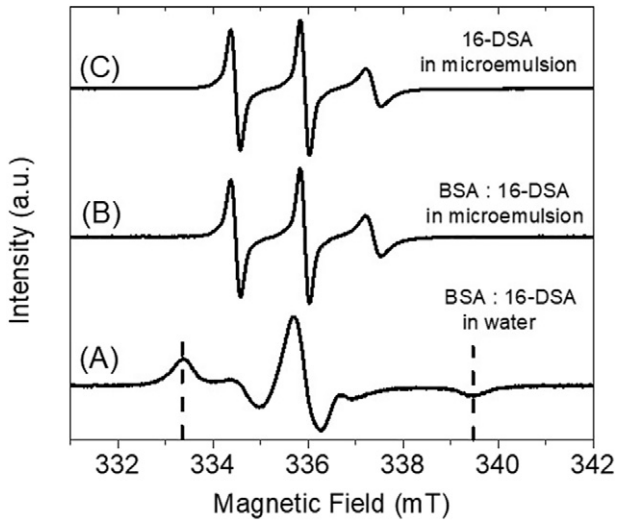

Fig. 4. CW EPR spectra of 16-DSA in BSA aqueous solution (A), 16-DSA/BSA complex in the water/Tween 20/$BmimPF_6$ microemulsion at 20:30:50%wt ratio (B), and 16-DSA in the same microemulsion without BSA (C). Dashed lines in (A) showed the characteristic signals of bound 16-DSA to BSA. The mol ratio of BSA:16-DSA is 1:2.

of 20:50:30. These sharper signals are signatures of the freely tumbling motion of 16-DSA. As a control experiment, the mixture of 16-DSA and microemulsion system without BSA was measured, and the almost same sharp signals coming from free 16-DSA radicals were obtained (Fig. 4(C)). The binding of both $BmimPF_6$ and Tween 20 to BSA have been previously studied. In the literature, the found binding constants of $BmimPF_6$ and Tween 20 to BSA are around 10^3 M^{-1} which is three-four orders of magnitude lower than the binding constant of stearic acid to BSA [51–53]. Therefore, replacement of 16-DSA by $BmimPF_6$ or Tween 20 could not be the reason of obtaining free 16-DSA. So, one can conclude that mixing of $BmimPF_6$/Tween 20 with BSA aqueous solution denatured the BSA protein and released the bound fatty acids.

In order to obtain albumin nanoparticles inside the water/Tween 20/$BmimPF_6$ microemulsion systems, a high-speed homogenizer was applied. As cross-linker, glutaraldehyde was added to the system to provide durability and stability to the BSA nanoparticles after homogenizer treatment. Fig. 5(A) shows the SEM image of BSA aggregates after only homogenizer treatment at 22,000 rpm. Since glutaraldehyde cross-linking was not used in this system, albumin formed undissolved micron-sized assemblies. On the other hand, homogenizer treatment at the same speed followed by glutaraldehyde addition yielded BSA NPs. Homogenizer speed is crucial for obtaining well dispersed nanoparticles. Without homogenizer treatment or low-speed homogenization at 8000 rpm leaded to micron-size BSA aggregates (Fig. 5(B, C)). DLS results also showed the hydrodynamic sizes of obtained BSA aggregates. Addition of glutaraldehyde to the system without high speed homogenization yielded larger aggregates with 1000 nm average size (Fig. 5(E-top)). Applying homogenizer at 8000 rpm resulted in BSA samples with a broad size distribution from 250 nm to a few micrometers (Fig. 5(E-middle)). Applying the homogenizer with the low speed to the viscous network might not be energetically successful to lead uniformly sized spherical nanoparticles. Viscosity and homogenization speed are directly related with the droplet size reduction in turbulence mechanism. The speed of homogenizer should be balanced with respect to the viscosity of medium to achieve intense collision between the water pools (Tween 20 molecules are aligned themselves at the interface) in the $BmimPF_6$ network. The applied powerful energy creates localized pressure differences with the eddies which tear apart water droplets into smaller droplets. Applying high-speed homogenizer at 22,000 rpm to water/IL was able to convert denatured BSA into spherical nanoparticles with the help of glutaraldehyde (SEM image in Fig. 5(D)). For SEM measurements, preparation of these soft nanomaterials could cause clustering during drying.

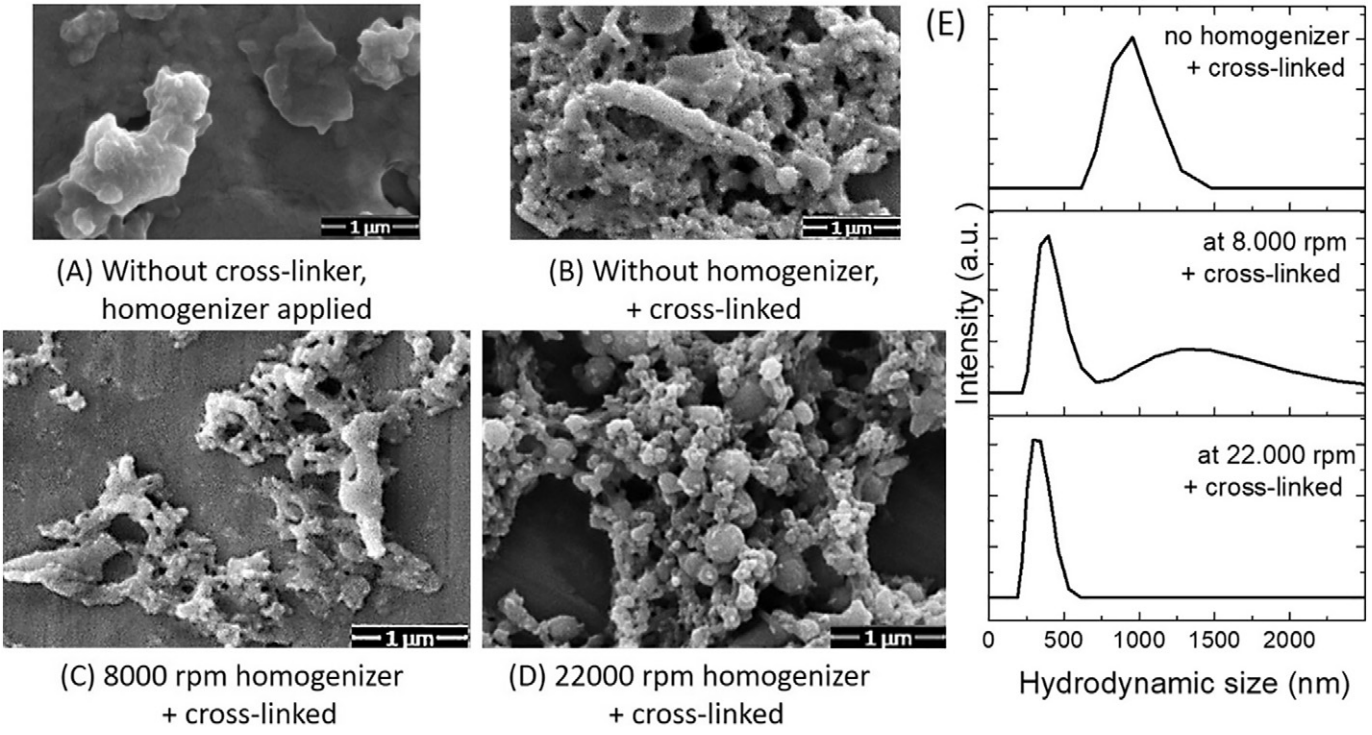

Fig. 5. Effects of using high-speed homogenizer and glutaraldehyde on the BSA NP preparation. SEM images of BSA samples prepared in the water/Tween 20/$BmimPF_6$ microemulsion with wt% of 5:75:20. (A) Homogenizer treatment was applied at 22,000 rpm without glutaraldehyde addition. Samples in (B–D) include glutaraldehyde: (B) without homogenizer treatment, (C) homogenizer treatment at 8000 rpm and (D) homogenizer treatment at 22,000 rpm. (E) DLS results of the same samples including glutaraldehyde (B–C).

Therefore, agglomerations were observed in Fig. 5(B)–(D). However, small spherical nanoparticles could be observed only in Fig. 5 (D) when the high speed homogenizer was applied. The DLS results also supported the SEM images. Using high speed homogenizer leaded to BSA nanoparticles with a narrow size distribution from 250 to 500 nm (Fig. 5(E-bottom)). Without using the homogenizer, larger particles around 1000 nm hydrodynamic size were detected by DLS. In addition, the zeta potential of the BSA nanoparticles was found as – 24 mV. The correlation between the results of SEM images (Fig. 5(A–D)) and DLS measurements (Fig. 5(E)) showed the necessities of high-speed homogenizer and glutaraldehyde together for resulting in the production of small-sized nanoparticles.

Although particle sizes can be determined using DLS or SEM techniques, their results especially for the soft nanomaterials could be different [54]. Since particles are measured in solution with DLS according to their hydration shell, it is reasonable to obtain higher average particle size compared to the SEM results. On the other hand, preparation of these soft nanomaterials for SEM measurements could cause clustering during drying. Fig. 6(A) showed the SEM image of BSA NPs synthesized in W/IL microemulsion containing another composition of water/Tween 20/$BmimPF_6$ with 20:50:30 wt%. The size distribution of spherical BSA NPs was obtained from the SEM image using ImageJ program (Fig. 6 (B)). The chosen spherical particles for the particle size analysis were shown in Fig. S4. BSA NPs of 103 nm average size with a size distribution between 60 and 260 nm was obtained from the SEM image. However, DLS provided their average hydrodynamic size as around 396 nm in solution with a PDI 0.367 (Fig. 6(C)). Obtaining smaller average particle size by SEM compared to DLS shows that dry and wet sizes of BSA NPs are significantly different which is in accordance with the other reported results [55–57]. The size discrepancy between DLS and SEM has various reasons. For example, sizes are measured indirectly by DLS and determined based on movement frequency of nanoparticles in solution [55]. But especially for soft nanomaterials, this discordance could be sourced from the swelling of the nanoparticles in the solution and this is a general problem in the literature [54,56,57]. Hence, swelling of nanoparticles in the solution, softness of the material, dynamic aggregation and movement in the solution, rigidity and amount of the surfactant film could affect the DLS measurement based on the used ratios.

3.3. Effect of surfactant and water concentrations on the BSA nanoparticle preparation

Surfactant molecules are necessary to reduce the interfacial tension between water and $BmimPF_6$ phases, and so to stabilize the nanosized water droplets in microemulsions. If the number of Tween 20 molecules is not sufficient with respect to the number of $BmimPF_6$, then the coalescence between water pools takes place to minimize the surface energy. This could also lead to form larger BSA NPs in the water pools. In the water/IL microemulsion region, BSA NPs could be synthesized using different Tween 20/$BmimPF_6$ weight ratios from 8.50 (85:10) to 0.27 (20:75). The corresponding mole ratios changed from 2:1 to 1:16. Fig. 7 shows the SEM images and DLS results of BSA NPs prepared in microemulsions with different Tween 20/$BmimPF_6$ mole ratios. At a constant water content (5 wt%), using an excess amount of Tween 20 (Tween 20/$BmimPF_6$, 2:1 mol ratio) yielded BSA NPs with a more uniform size distribution. The SEM image revealed the formation of BSA NPs with 100–200 nm particle sizes (Fig. 7(A), down). Also, DLS provided their average hydrodynamic size as 400 nm in solution with a

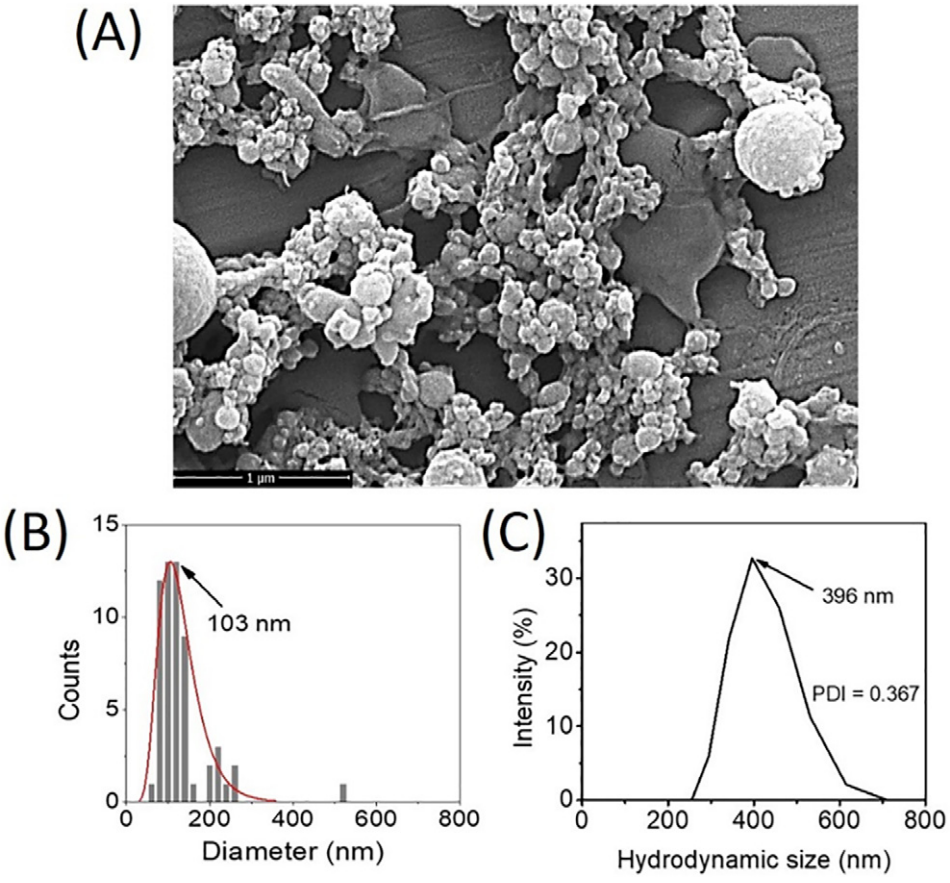

Fig. 6. (A) SEM image of BSA NPs prepared in the water/Tween 20/$BmimPF_6$ microemulsion with wt% of 20:50:30. (B) Particle size distribution obtained from the SEM image (A). (C) DLS hydrodynamic size distribution of BSA NPs.

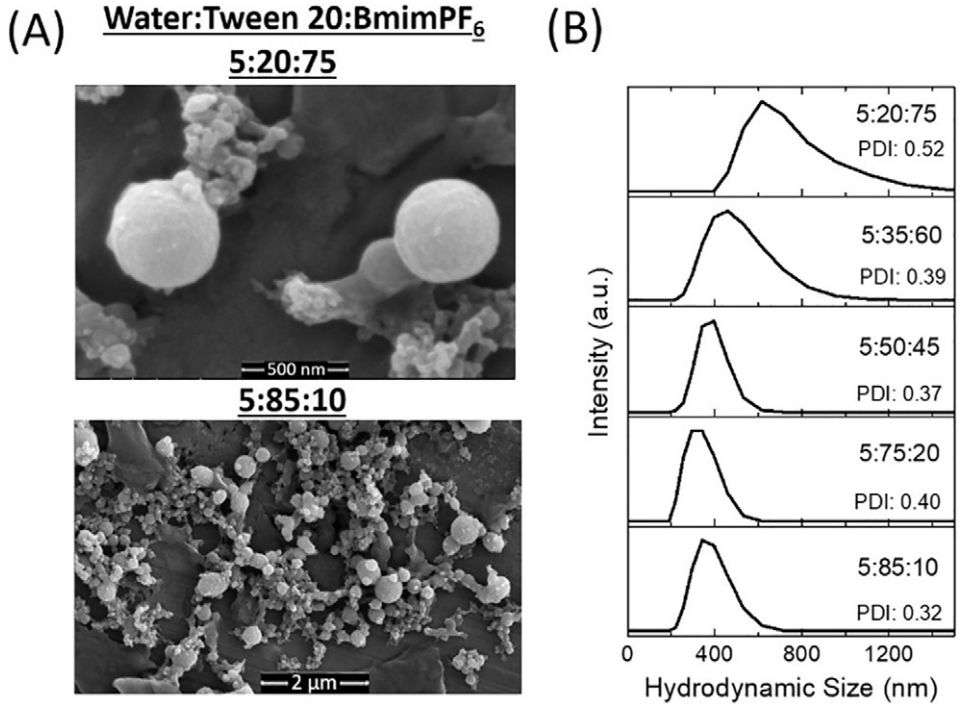

Fig. 7. (A) SEM images of BSA NPs prepared in the water/Tween 20/$BmimPF_6$ microemulsions with wt% of 5:20:75 (top) and 5:85:10 (down), and their corresponding Tween 20/$BmimPF_6$ mole ratios are 1:16 (top) and 2:1 (down), and (B) DLS results of hydrodynamic size distributions of BSA NPs prepared in different water/Tween 20/$BmimPF_6$ microemulsions with the constant water concentration (5 wt%).

PDI 0.32. On the other hand, using a lower Tween 20/$BmimPF_6$ mole ratio (1:16) yielded a limited number of BSA NPs around 500 nm particle size (Fig. 7(A), top). DLS results also supported SEM image with an average particle size of 600 nm and a larger PDI 0.52. In addition, the broad size distribution obtained by the DLS reveals the instability of nanoparticles in the dispersion when a limited number of Tween 20 was used. Since nano-sized water droplets are used as nanoreactors to prepare inorganic or polymeric nanoparticles in the water-in-oil microemulsions, size and shape of water droplets are important to get the desired size and shape of nanoparticles.

Especially for the synthesizing of inorganic nanomaterials, increasing the water content increases the size of nanoparticles [16]. However, water content is not the only parameter to control the nanoparticle size. Other control parameters e.g. types and concentrations of oil, surfactant and co-surfactant, and the flexibility of surfactant molecules affect the final size of the nanoparticles.

Here, a broad range of water content between 2 and 30 wt% was used to prepare BSA NPs inside the water droplets of different W/IL microemulsions. Table 1 shows the chosen composition fractions of W/IL microemulsions in which water content varies while keeping the surfactant or IL contents constant. Fig. 8 shows the DLS and SEM results of BSA NPs prepared in W/IL microemulsions. From DLS measurements, at constant Tween 20 concentration (50 wt%) or at constant $BmimPF_6$ concentration (20 wt%), changing the water content from 2 wt% to 30 wt% yielded similar average size BSA NPs around 350–450 nm. The PDI results of DLS measurements were between 0.25 and 0.58. The nanoparticle size distribution became broader when 30 wt% of water was used. This result is in accordance with the obtaining a broader size distribution of water droplets without BSA when 30 wt% of water content was used (Fig. 3). In addition, SEM results of BSA nanoparticles showed that increasing the water content in the microemulsion did not affect the size of BSA NPs significantly. Moreover, using another nonionic surfactant TX-100 instead of Tween 20 in the preparation of BSA NPs yielded comparable results. In Fig. S5, SEM and DLS results showed that BSA NPs prepared in the water/Tween 20/$BmimPF_6$ or in the water/TX 100/$BmimPF_6$ microemulsions with wt% of 5:50:45 had similar sizes with similar size distributions.

3.4. Cellular uptake of BSA NPs

The uptake of BSA NPs by Huh7 cells was studied using confocal microscope (Fig. 9(A–D)). For the cellular uptake experiments, fluorescein isothiocyanate (FITC) labeled BSA was used to visualize the distribution of BSA NPs. FITC-BSA nanoparticles were prepared inside the water/Tween 20/$BmimPF_6$ microemulsion system with wt% of 20:50:30. At a concentration of 0.1 mg/mL, FITC-BSA NPs were mostly distributed inside the cell after incubation times of 4 and 24 h. In addition, folate conjugated BSA NPs were prepared to study the intracellular nanoparticle uptake. Previously, it has been shown that conjugation of folic acid to serum albumin nanoparticles increased nanoparticles uptake into cancer cell lines; the human neuroblastoma (UKF-NB-3) and the rat glioblastoma (101/8) due to the elevated expression of the folate receptors in various types of human cancers [40,58]. However, here folate conjugation did not increase BSA nanoparticles binding to Huh7 cells. Both nonmodified and folate conjugated BSA NPs were uptaken by Huh7 cells extensively (Fig. 9(A–D)).

3.5. Cell viability

$BmimPF_6$ involved in the preparation of BSA nanoparticles exhibits cytotoxicity when cell is directly exposed to the $BmimPF_6$. In the literature, it has been shown that the half maximal effective concentration (EC_{50}) value of imidazolium based ILs decreases with increasing the alkyl side chain length of the imidazolium ring, while the anion has a low effect on the EC_{50} [59]. For example, the reported log EC_{50} values of C_4mimPF_6, C_6mimPF_6 and C_8mimPF_6 are 3.07, 2.17 and 0.95 μM, respectively. Here, $BmimPF_6$ (C_4mimPF_6) was used as continuous phase in microemulsion instead of conventional organic

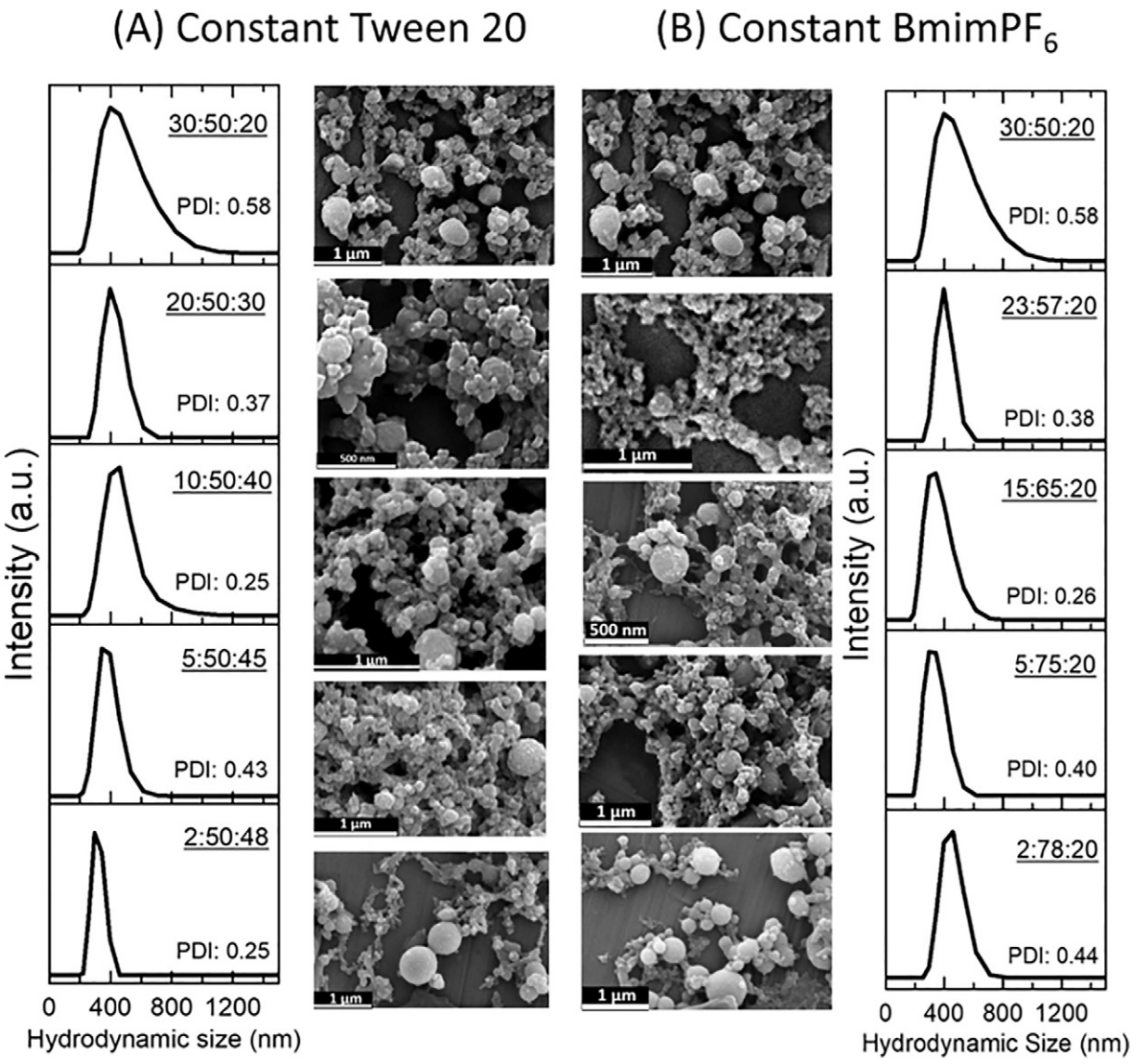

Fig. 8. DLS results and SEM images of BSA NPs prepared in the series of different water/Tween 20/$BmimPF_6$ microemulsions at constant wt% of Tween 20 (A) and at constant wt% of $BmimPF_6$ (B). The wt% order is water:Tween 20:$BmimPF_6$.

solvents e.g. DCM (EC_{50}: 4.07–4.53), benzene (EC_{50}: 1.41–3.12) or chloroform (EC_{50}: 3.55–4.32). Therefore, the cytotoxicity of $BmimPF_6$ is not expected to be so different than the cytotoxicities of these volatile organic solvents. To avoid $BmimPF_6$, albumin nanoparticles were centrifuged and purified a few times. For Huh7 cells, cellular uptake of BSA NPs or folic acid conjugated BSA NPs had no significant influence on cell viability up to 4 mg/mL concentrations for 24 h and 48 h (Fig. 9(E–F)). Therefore, BSA NPs prepared in the water-in-$BmimPF_6$ microemulsions over a broad concentration range could be used for future drug delivery studies without affecting the cell viability.

4. Conclusions

Here we showed that albumin nanoparticles can be prepared in water-in-IL microemulsion system with help of high-speed homogenizer and glutaraldehyde as cross-linker. As an alternative to conventional organic volatile solvents, a green solvent of $BmimPF_6$ was used in preparation of microemulsions. Dispersed nano-sized water droplets inside the microemulsion behave like a nanoreactor to prepare BSA NPs. Increasing water content from 2 wt% to 30 wt% significantly increased water droplets sizes but not the sizes of formed BSA NPs. On the other hand, using a higher surfactant/IL weight ratio stabilized the formed albumin nanoparticles with a narrower size distribution. This showed the importance of surfactant molecules in stabilization of nanoparticles in microemulsions. By systematically changing the weight ratios of microemulsion components, BSA NPs of 103 nm average size with a size distribution between 60 and 260 nm were obtained. Moreover, their high cellular uptake ability and no influence on cell viability showed that BSA nanoparticles prepared with this technique could be used in drug delivery studies.

Acknowledgment

This work was financially supported by Scientific and Technological Research Council of Turkey (Tubitak) via 1001 Program under grant 118Z341. Authors thank Barış Yıldırım for his help preparing the phase diagram. Authors thank IZTECH Center for Materials Research and Biotechnology and Bioengineering Research Center, and Izmir Biomedicine and Genome Center Optic Imaging Core Facility.

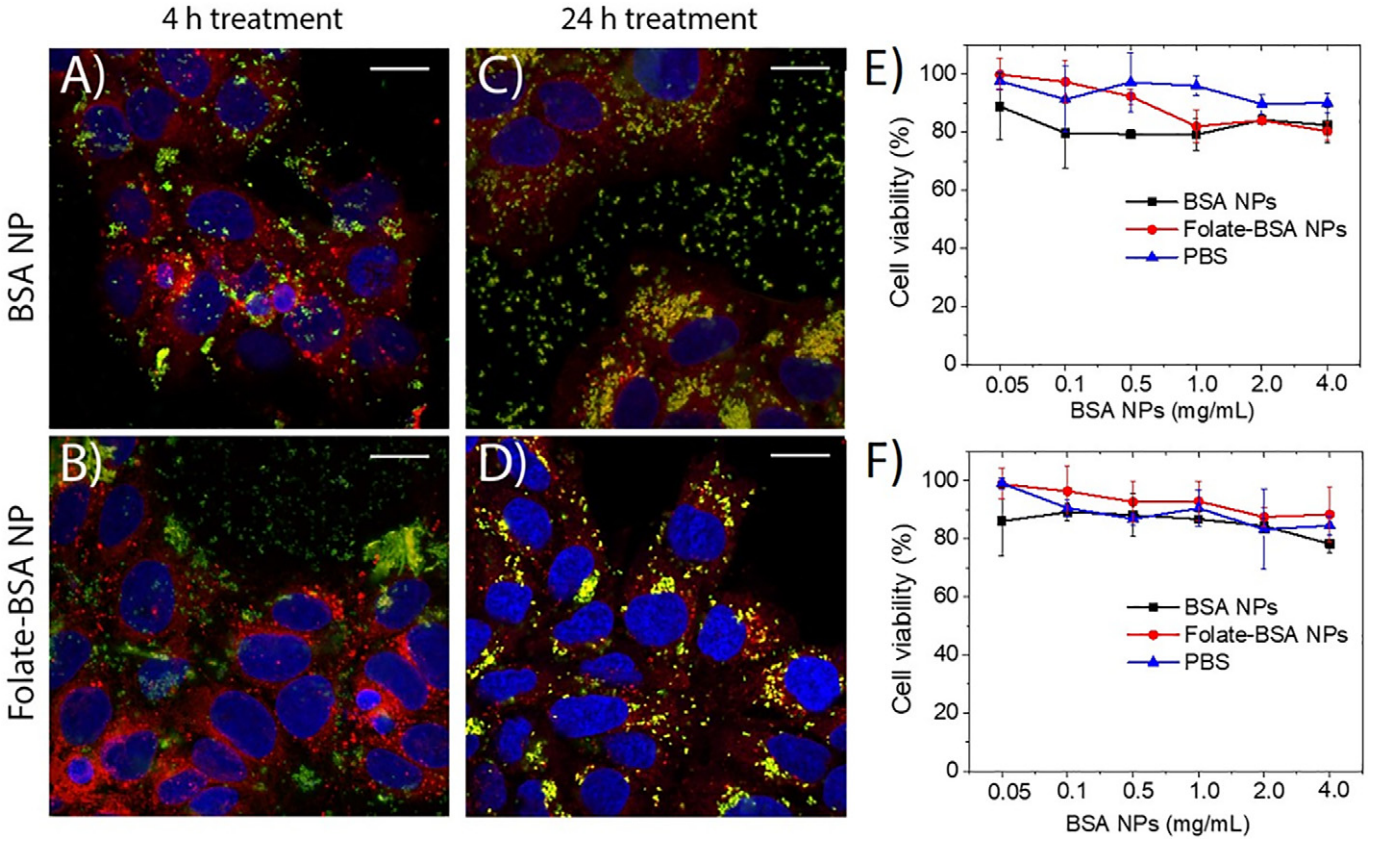

Fig. 9. Huh7 cells were treated for 4 h (A–B) and 24 h (C–D) with 0.1 mg/mL non modified (top) or folate conjugated (bottom) FITC-BSA NPs. Cell membranes are stained with DiI (red) and nuclei are stained with DAPI (blue). Scale bar = 20 μm. (E–F) Cell viability of nonmodified and folate modified BSA nanoparticles, and also PBS as reference. The cells were incubated with different concentrations of nanoparticles: 0.05, 0.1, 0.5, 1.0, 2.0, 4.0 mg/mL for 24 h (E) and 48 h (F) incubation times.

Appendix A. Supplementary data

Supplementary data to this article can be found online at https://doi.org/10.1016/j.molliq.2019.111713.

References

[1] T. Welton, Room-temperature ionic liquids. Solvents for synthesis and catalysis, Chem. Rev. 99 (1999) 2071–2084.
[2] Q. Zhang, S. Zhang, Y. Deng, Recent advances in ionic liquid catalysis, Green Chem. 13 (2011) 2619–2637.
[3] D.S. Silvester, R.G. Compton, Electrochemistry in room temperature, ionic liquids: a review and some possible applications, Z. Phys. Chem. 220 (2006) 1247–1274.
[4] N.V. Plechkovaa, R.S. Kenneth, Applications of ionic liquids in the chemical industry, Chem. Soc. Rev. 37 (2008) 123–150.
[5] B. Sasikumar, G. Arthanareeswaran, A.F. Ismail, Recent progress in ionic liquid membranes for gas separation, J. Mol. Liq. 266 (2018) 330–341.
[6] Z. Qiu, J. Texter, Ionic liquids in microemulsions, Curr. Opin. Colloid Interface Sci. 13 (2008) 252–262.
[7] J. Kuchlyan, N. Kundu, N. Sarkar, Ionic liquids in microemulsions: formulation and characterization, Curr. Opin. Colloid Interface Sci. 25 (2016) 27–38.
[8] J.H. Porada, M. Mansueto, S. Laschat, C. Stubenrauch, Microemulsions with hydrophobic ionic liquids: influence of the structure of the anion, J. Mol. Liq. 227 (2017) 202–209.
[9] J. Eastoe, S. Gold, S.E. Rogers, A. Paul, T. Welton, R.K. Heenan, I. Grillo, Ionic liquid-in-oil microemulsions, J. Am. Chem. Soc. 127 (2005) 7302–7303.
[10] R. Rai, S. Pandey, Evidence of water-in-ionic liquid microemulsion formation by nonionic surfactant Brij-35, Langmuir 30 (2014) 10156–10160.
[11] Y. Gao, S. Han, B. Han, G. Li, D. Shen, Z. Li, J. Du, W. Hou, G. Zhang, TX-100/water/1-butyl-3-methylimidazolium hexafluorophosphate microemulsions, Langmuir 21 (2005) 5681–5684.
[12] M. Moniruzzaman, N. Kamiya, K. Nakashima, M. Goto, Formation of reverse micelles in a room-temperature ionic liquid, ChemPhysChem 9 (2008) 689–692.
[13] N. Adawiyah, M. Moniruzzaman, S. Hawatulaila, Goto, Ionic liquids as a potential tool for drug delivery systems, Med. Chem. Commun. 7 (2016) 1881–1897.
[14] M.A. Malik, M.Y. Wani, M.A. Hashim, Microemulsion method: a novel route to synthesize organic and inorganic nanomaterials, Arab. J. Chem. 5 (2012) 397–417.
[15] A.K. Ganguli, A. Ganguly, S. Vaidya, Microemulsion-based synthesis of nanocrystalline materials, Chem. Soc. Rev. 39 (2010) 474–485.
[16] B. Richard, J.-L. Lemyre, A.M. Ritcey, Nanoparticle size control in microemulsion synthesis, Langmuir 33 (2017) 4748–4757.
[17] X. Wang, J. Cheng, G. Ji, X. Peng, Z. Luo, Starch nanoparticles prepared in a two ionic liquid based microemulsion system and their drug loading and release properties, RSC Adv. 6 (2016) 4751–4757.
[18] R. Ranjan, S. Vaidya, P. Thaplyal, M. Qamar, J. Ahmed, A.K. Ganguli, Controlling the size, morphology, and aspect ratio of nanostructures using reverse micelles: a case study of copper oxalate monohydrate, Langmuir 25 (2009) 6469–6475.
[19] M. Zhao, L. Zheng, X. Bai, N. Li, L. Yu, Fabrication of silica nanoparticles and hollow spheres using ionic liquid microemulsion droplets as templates, Colloids Surf. A Physicochem. Eng. Asp. 346 (2009) 229–236.
[20] F. Yan, J. Texter, Surfactant ionic liquid-based microemulsions for polymerization, Chem. Commun. (2006) 2696–2698.
[21] C. Fu, H. Zhou, D. Xie, L. Sun, Y. Yin, J. Chen, Y. Kuang, Electrodeposition of gold nanoparticles from ionic liquid microemulsion, Colloid Polym. Sci. 288 (2010) 1097–1103.
[22] G. Zhou, Z. Luo, X. Fu, Preparation of starch nanoparticles in a water-in-ionic liquid microemulsion system and their drug loading and releasing properties, J. Agric. Food Chem. 62 (2014) 8214–8220.
[23] G. Zhou, Z. Luo, X. Fu, Preparation and characterization of starch nanoparticles in ionic liquid-in-oil microemulsions system, Ind. Crop. Prod. 52 (2014) 105–110.
[24] B. Demirkurt, Y. Akdogan, Development of an ionic liquid based method for the preparation of albumin nanoparticles, ChemistrySelect 3 (2018) 9940–9945.
[25] D.R. Kattnig, Y. Akdogan, I. Lieberwirth, D. Hinderberger, Spin probing of supramolecular structures in 1-butyl-3-methyl-imidazolium tetrafluoroborate/water mixtures, Mol. Phys. 111 (2013) 2723–2737.
[26] D.R. Kattnig, Y. Akdogan, C. Bauer, D. Hinderberger, High-field EPR spectroscopic characterization of spin probes in aqueous ionic liquid mixtures, Z. Phys. Chem. 226 (2012) 1363–1378.
[27] K. Saihara, Y. Yoshimura, S. Ohta, A. Shimizu, Properties of water confined in ionic liquids, Sci. Rep. 5 (2015) 10619.
[28] T. Peters, All About Albumin: Biochemistry, Genetics and Medical Applications, Academic Press, San Diego, 1995.
[29] N. Lomis, S. Westfall, L. Farahdel, M. Malhotra, D. Shum-Tim, S. Prakash, Human serum albumin nanoparticles for use in cancer drug delivery: process optimization and in vitro characterization, Nanomaterials 6 (2016) 1–17.

[30] X. Tang, G. Wang, S. Shi, K. Jiang, L. Meng, H. Ren, J. Wu, Y. Hu, Enhanced tolerance and antitumor efficacy by docetaxel-loaded albumin nanoparticles, Drug Deliv. 23 (2016) 2686–2696.
[31] A.O. Elzoghby, W.M. Samy, N.A. Elgindy, Albumin-based nanoparticles as potential controlled release drug delivery systems, J. Control. Release 157 (2012) 168–182.
[32] K. Langer, S. Balthasar, V. Vogel, N. Dinauer, H. Von Briesen, D. Schubert, Optimization of the preparation process for human serum albumin (HSA) nanoparticles, Int. J. Pharm. 257 (2003) 169–180.
[33] B. Von Storp, A. Engel, A. Boeker, M. Ploeger, K. Langer, Albumin nanoparticles with predictable size by desolvation procedure, J. Microencapsul. 29 (2012) 138–146.
[34] K.R. Shankar, R.K. Ameta, M. Singh, Preparation of BSA nanoparticles using aqueous urea at T = 308.15, 313.15 and 318.15 K as a function of temperature, J. Mol. Liq. *216* (2016) 808–813.
[35] L. Yang, F. Cui, D. Cun, A. Tao, K. Shi, W. Lin, Preparation, characterization and biodistribution of the lactone form of 10-hydroxycamptothecin (HCPT)-loaded bovine serum albumin (BSA) nanoparticles, Int. J. Pharm. 340 (2007) 163–172.
[36] F. Crisante, I. Francolini, M. Bellusci, A. Martinelli, L. D'Ilario, A. Piozzi, Antibiotic delivery polyurethanes containing albumin and polyallylamine nanoparticles, Eur. J. Pharm. Sci. 36 (2009) 555–564.
[37] Q. Zhang, L. Zhang, L. Zemin, X. Xie, X. Gao, X. Xu, Inducing controlled release and increased tumor-targeted delivery of chlorambucil via albumin/liposome hybrid nanoparticles, AAPS PharmSciTech 18 (2017) 2977–2986.
[38] Y. Gao, N. Li, L. Zheng, X. Zhao, S. Zhang, B. Han, W. Hou, G. Li, A cyclic voltammetric technique for the detection of micro-regions of bmimPF6/Tween 20/H2O microemulsions and their performance characterization by UV-Vis spectroscopy, Green Chem. 8 (2006) 43–49.
[39] B. Dong, S. Zhang, L. Zheng, J. Xu, Ionic liquid microemulsions: a new medium for electropolymerization, J. Electroanal. Chem. 619-620 (2008) 193–196.
[40] K. Ulbrich, M. Michaelis, F. Rothweiler, T. Knobloch, P. Sithisarn, J. Cinatl, J. Kreuter, Interaction of folate-conjugated human serum albumin (HSA) nanoparticles with tumour cells, Int. J. Pharm. 406 (2011) 128–134.
[41] R.P. Swatloski, A.E. Visser, W.M. Reichert, G.A. Broker, L.M. Farina, J.D. Holbrey, R.D. Rogers, On the solubilization of water with ethanol in hydrophobic hexafluorophosphate ionic liquids, Green Chem. 4 (2002) 81–87.
[42] C. Samori, Ionic liquids and their biological effects towards microorganisms, Curr. Org. Chem. 15 (2**011**) 1888–1904.
[43] Q. Li, X. Huang, Formation of 1-butyl-3-methylimidazolium bis(2-ethyl-1-hexyl) sulfosuccinate stabilized water-in-1-butyl-3-methylimidazolium bis (trifluoromethanesulfonyl)imide microemulsion and the effects of additives, J. Solut. Chem. 46 (2017) 1792–1804.
[44] G. Ji, Z. Luo, Z. Xiao, X. Peng, Synthesis of starch nanoparticles in a novel microemulsion with two ILs substituting two phases, J. Mater. Sci. 51 (2016) 7085–7092.
[45] D. Attwood, G. Ktistis, A light scattering study on oil-in-water microemulsions, Int. J. Pharm. 52 (1989) 165–171.
[46] S.T. Hyde, Hand Book of Applied Surface and Colloid Chemistry, Wiley, New York, 2001 299–332.
[47] L.R.S. Barbosa, M.G. Ortore, F. Spinozzi, P. Mariani, S. Bernstorff, R. Itri, The importance of protein-protein interactions on the pH-induced conformational changes of bovine serum albumin: a small-angle X-ray scattering study, Biophys. J. 98 (2010) 147–157.
[48] Y. Akdogan, M.J.N. Junk, D. Hinderberger, Effect of ionic liquids on the solution structure of human serum albumin, Biomacromolecules 12 (2011) 1072–1079.
[49] Y. Akdogan, D. Hinderberger, Solvent-induced protein refolding at low temperatures, J. Phys. Chem. B 115 (2011) 15422–15429.
[50] Y. Akdogan, M. Emrullahoglu, D. Tatlidil, M. Ucuncu, G. Cakan-Akdogan, EPR studies of intermolecular interactions and competitive binding of drugs in a drug–BSA binding model, Phys. Chem. Chem. Phys. 18 (2016) 22531–22539.
[51] L.-Y. Zhu, G.-Q. Li, F.-Y. Zheng, Interaction of bovine serum albumin with two alkylimidazolium-based ionic liquids investigated by microcalorimetry and circular dichroism, J. Biophys. Chem. 2 (2011) 146–151.
[52] P. Garidel, C. Hoffmann, A. Blume, A thermodynamic analysis of the binding interaction between polysorbate 20 and 80 with human serum albumins and immunoglobulins: a contribution to understand colloidal protein stabilization, Biophys. Chem. 143 (2009) 70–78.
[53] A. Varshney, P. Sen, E. Ahmad, M. Rehan, N. Subbarao, R.H. Khan, Ligand binding strategies of human serum albumin: how can the cargo be utilized? Chirality 22 (2010) 77–87.
[54] M.G. Montalbán, G. Carissimi, A.A. Lozano-Pérez, J.L. Cenis, J.M. Coburn, D.L. Kaplan, G. Víllora, Biopolymeric nanoparticle synthesis in ionic liquids, IntechOpen (2018) 3–26, https://doi.org/10.5772/intechopen.78766.
[55] P. Eaton, P. Quaresma, C. Soares, C. Neves, M.P. de Almeida, E. Pereira, P. West, A direct comparison of experimental methods to measure dimensions of synthetic nanoparticles, Ultramicroscopy 182 (2017) 179–190.
[56] Y.-Q. Zhang, W.-D. Shen, R.-L. Xiang, L.-J. Zhuge, W.-J. Gao, W.-B. Wang, Formation of silk fibroin nanoparticles in water-miscible organic solvent and their characterization, J. Nanopart. Res. 9 (2007) 885–900.
[57] L. Xiao, G. Lu, Q. Lu, D.L. Kaplan, Direct formation of silk nanoparticles for drug delivery, ACS Biomater Sci. Eng. 2 (2016) 2050–2057.
[58] C.P. Leamon, Folate-targeted drug strategies for the treatment of cancer, Curr. Opin. Investig. Drugs 9 (2008) 1277–1286.
[59] A. Romero, A. Santos, J. Tojo, A. Rodriguez, Toxicity and biodegradability of imidazolium ionic liquids, J. Hazard. Mater. 151 (2008) 268–273.